RSC Advances

PAPER

View Article Online
View Journal | View Issue

Cite this: *RSC Adv.*, 2020, **10**, 4201

Electronic and optical properties of monolayer MoS_2 under the influence of polyethyleneimine adsorption and pressure

Ong Kim Le,[a] Viorel Chihaia,[b] My-Phuong Pham-Ho*[ac] and Do Ngoc Son*[a]

MoS_2 is one of the well-known transition metal dichalcogenides. The moderate bandgap of monolayer MoS_2 is fascinating for the new generation of optoelectronic devices. Unfortunately, MoS_2 is sensitive to gases in the environment causing its original electronic properties to be modified unexpectedly. This problem has been solved by coating MoS_2 with polymers such as polyethyleneimine (PEI). Furthermore, the application of pressure is also an effective method to modify the physical properties of MoS_2. However, the effects of polyethyleneimine and pressure on the electronic and optical properties of monolayer MoS_2 remain unknown. Therefore, we elucidated this matter by using density functional theory calculations. The results showed that the adsorption of the PEI molecule significantly reduces the width of the direct bandgap of the monolayer MoS_2 to 0.55 eV because of the occurrence of the new energy levels in the bandgap region due to the contribution of the N-$2p_z$ state of the PEI molecule. Remarkably, the transition from semiconductor to metal of the monolayer MoS_2 and the MoS_2/PEI system occurs at the tensile pressure of 24.95 and 21.79 GPa, respectively. The bandgap of these systems approaches 0 eV at the corresponding pressures. Importantly, new peaks in the optical spectrum of the clean MoS_2 and MoS_2/PEI appear in the ultraviolet region under compressive pressures and the infrared region under tensile strains.

Received 1st November 2019
Accepted 19th January 2020

DOI: 10.1039/c9ra09042h

rsc.li/rsc-advances

1. Introduction

MoS_2 is one of the most often studied transition metal dichalcogenides (TMDs)[1–24] due to the convergence of many advanced properties for optical,[1] electronic,[2] and mechanical[3] applications. Similar to graphene, the bonding between the layers of MoS_2 is the weak van der Waals interaction. Therefore, the monolayer of MoS_2 can be fabricated by exfoliation, which has a thickness of about 0.65 nm. In particular, the monolayer MoS_2 has a direct bandgap of *ca.* 1.8 eV,[4] which makes this material suitable for transistors,[5] photodetectors, and light-emitting diodes.[6] Field-effect transistors (FETs) of monolayer MoS_2 demonstrated a high on/off current ratio exceeding 10^8 and the electron mobility of at least 200 $cm^2 V^{-1} s^{-1}$.[5] The main problem of MoS_2 is that it is sensitive to oxygen gas in air, which modifies its electronic properties unexpectedly. Thus, the bandgap becomes narrower and even disappeared after a few days of exposure to oxygen gas.[7] To solve this problem, the dichalcogenide can be covered with polymers such as polyethyleneimine (PEI).[8,9]

Furthermore, control of the electronic and optical properties of the monolayer MoS_2 by changing the crystal structure,[10] layer thickness,[4] and applying strain[11] was achieved. The results showed that the homogeneous biaxial tensile strain of around 10% led to the semiconductor-to-metal transition in all semiconducting TMDs.[12] Several theoretical and experimental studies showed that the bandgap of the monolayer MoS_2 decreases as the tensile strain increases,[12,13] while it is a parabola for compression.[14–17] Fan *et al.* demonstrated that the bandgap at the K point changes from direct to indirect with compressive pressure.[14] Generally, the influence on the electronic structure properties of monolayer MoS_2 depends on the type of applied strain. Experimentally, it is difficult to exert a homogeneous hydrostatic strain on a 2D material sample and can only generate a biaxial compressive strain up to 0.2% with elaborate setups.[18] In a recent study, the monolayer MoS_2 was investigated under extreme hydrostatic pressures of up to 30 GPa. Although a higher pressure is not experimentally achievable at present, a metallization at the compressive pressure of 68 GPa was predicted by theoretical calculations.[19] In addition to the ability to tune the electronic properties of the monolayer MoS_2, the applied strain was found to modify the photoluminescence (PL) intensity. The PL maximum peak of the monolayer MoS_2 exhibited a blue shift[20,21] at the rate of

[a]*Ho Chi Minh City University of Technology, VNU-HCM, 268 Ly Thuong Kiet Street, District 10, Ho Chi Minh City, Vietnam. E-mail: phmphuong@hcmut.edu.vn; dnson@hcmut.edu.vn*

[b]*Institute of Physical Chemistry "Ilie Murgulescu" of the Romanian Academy, Splaiul Independentei 202, Sector 6, 060021 Bucharest, Romania*

[c]*Institute for Computational Science and Technology, Quang Trung Software City, SBI Building, Street No. 3, Tan Chanh Hiep Ward, District 12, Ho Chi Minh City, Vietnam*

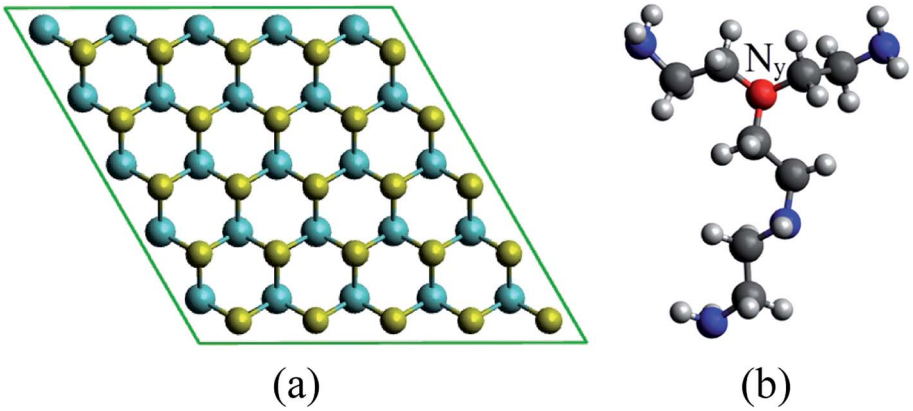

Fig. 1 The optimized structures of (a) the monolayer MoS_2 and (b) the truncated-branched PEI molecule. Cyan, yellow, grey, blue, and white colors represent Mo, S, C, N, and H atoms, respectively. Here, the N_y symbol denotes the N atom (red color) with three alkyl groups.

approximately 20 meV GPa^{-1}. At the pressure of 25 GPa, both real and imaginary parts of the dielectric function were shifted to red, and the peak height increases correspondence with an enhancement of the optical absorption.[21] These results demonstrated that one can adjust the electronic and optical properties of MoS_2 by applying pressures. Interestingly, the monolayer MoS_2 phototransistor exhibited a better photoresponsivity compared to the graphene-based devices.[22]

The effects of organic molecules adsorption such as TCNQ, TCNE, TTF, BV, F4TCNQ, and benzene on the electronic and optical properties of the monolayer MoS_2 have been studied in the literature.[23–26] A reduction of the bandgap was found due to the existence of the flat molecular levels of the organic molecules in the bandgap region of the monolayer MoS_2. The theoretical study showed that the adsorption of TCNQ significantly enhances the peak height of the optical absorption of the monolayer MoS_2 in the infrared region of the spectrum.[23,24] Du *et al.* experimentally studied the adsorption of the PEI on multilayer MoS_2 field-effect transistors.[8] The experimental results demonstrated that a reduction of 2.6 times in sheet resistance and 1.2 times in contact resistance have been achieved. The enhancement of electrical properties was reflected in an improvement of 70% for ON-current and 50% for extrinsic field-effect mobility. Our previous study showed that the

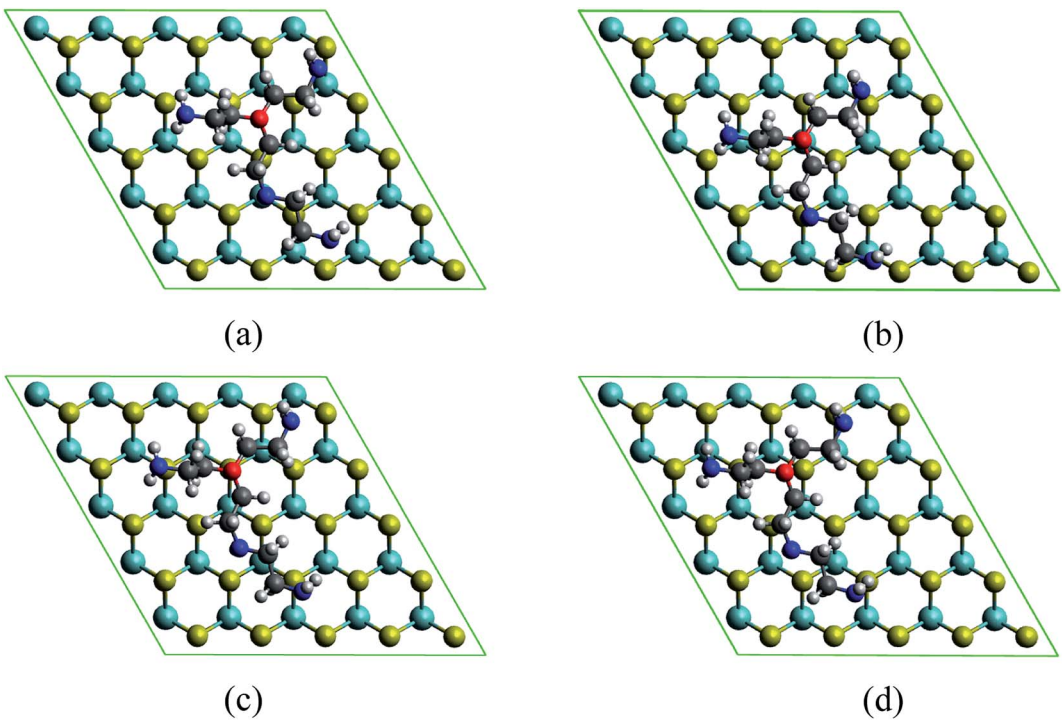

Fig. 2 The favorable adsorption sites of the PEI molecule on the MoS_2 monolayer when the N_y nitrogen atom over the hollow site (a), the molybdenum atom (b), the sulfur atom (c), and the bridge site of two S atoms (d).

Table 1 Adsorption energy E_a, the distances d_{N-S}, d_{C-S}, and d_{H-S} (Å) from the nearest atoms of the PEI fragment to the monolayer MoS_2 with the change of lattice constant a

a (Å)	E_a (eV)	d_{N-S} (Å)	d_{C-S} (Å)	d_{H-S} (Å)
2.84	0.139	3.53	3.63	2.26
3.00	0.063	3.57	3.72	2.30
3.18	−0.007	3.63	3.76	2.37
3.32	−0.085	3.68	3.81	2.42
3.48	−0.315	3.73	3.88	2.46
3.64	−0.479	3.83	3.93	2.51

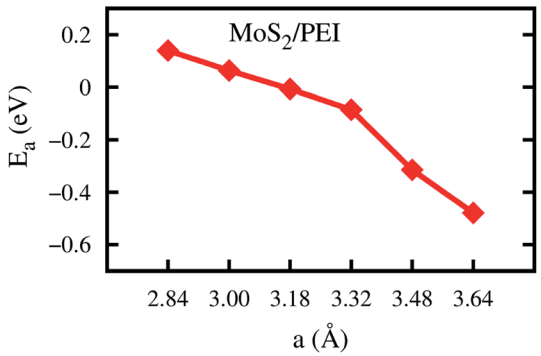

Fig. 3 The adsorption energy of the PEI fragment on the monolayer MoS_2 as a function of the lattice constant.

adsorption of the PEI molecule enhances the luminescence ability of the multi-layer MoS_2 FET from 0.14 to 4.41 AW^{-1}.[9] However, the influences of both pressure and the PEI adsorption on the electronic and optical properties of MoS_2 remain unknown. Therefore, in the present work, we are going to clarify this matter by using the density functional theory calculations.

1.1. Computational method

We used density functional theory calculations with the aid of the Vienna *ab initio* simulation package.[27–29] The Perdew–Burke–Ernzerhof version of the generalized gradient approximation (GGA-PBE) was utilized for the exchange-correlation energy.[30,31] The calculations of the band structure of monolayer MoS_2 using various schemes have been summarized in the literature.[32] The GGA functional plus van der Waals corrections underestimate the bandgap, while GW correction and HSE06 functional overestimate it. Local density approximation and GGA-PBE methods offered the most reasonable band gaps. Considering this result, as well as the accuracy in the geometries obtained by the GGA-PBE functional, in this study we used this functional to determine the effects of PEI doping on the MoS_2 surface. The projector-augmented-wave method was taken into account for the electron–ion interactions.[33,34] The plane-wave basis set was expanded with the cutoff energy of 600 eV. The surface Brillouin zone integration was performed by using the special k-point sampling technique of Monkhorst–Pack[35] with the k-point mesh of $3 \times 3 \times 1$. We also included the dipole corrections[36,37] in the simulation for a periodic supercell to correct the interaction between the repeated images. The Gaussian smearing of order 0 with the sigma value of 0.1 was used to speed up the convergence of the calculations. The monolayer MoS_2 (Fig. 1a) was modeled by the supercell approach using the 5×5 unit cell with the vacuum space of 16 Å along the z-direction. The vacuum space has been checked to make sure of no significant interaction of repeating images of the supercell. The truncated branched PEI fragment (Fig. 1b) was constructed based on the following requirements:[9] (1) the total charge of the fragment is neutral, (2) the structure of the truncated fragment should contain nitrogen atoms accompany with one, two, and three alkyl groups. All atoms were allowed to fully relax during the geometry optimization until the Hellmann–Feynman force acting on each atom was less than 0.001 eV $Å^{-1}$. Spin-polarized calculations were performed for the geometry optimization and the calculation of band structure.

Adsorption energy was calculated to understand the binding strength of the PEI fragment on MoS_2 through the formula:

$$E_a = E_{sub+PEI} - (E_{sub} + E_{PEI}), \quad (1)$$

where $E_{sub+PEI}$ is the total energy of the MoS_2 + PEI system. The total energy of the monolayer MoS_2 and that of the isolated PEI fragment are denoted as E_{sub} and E_{PEI}, respectively.

The pressure was estimated from the energy cost over the change of volume by:[19]

$$P = \frac{E - E_0}{V - V_0}, \quad (2)$$

here, E and V (E_0 and V_0) are the energy and volume of the strained (unstrained) system, respectively. The unit cell volume of the hexagonal lattice of the MoS_2 was calculated by $V = \frac{\sqrt{3}}{2}a^2c$, where a is the lattice constant and c is the thickness of the slab. We perform the modification of pressure by

Table 2 The structural parameters of the MoS_2 monolayer with the change of lattice constant. See Fig. 4 for the atom index of MoS_2

a (Å)		2.84	3.00	3.18	3.32	3.48	3.64
Average bond length (Å)	S_1–S_2	2.85	3.06	3.18	3.32	3.48	3.57
	S_1–S_3	3.38	3.26	3.13	3.05	2.95	2.88
	Mo_1–Mo_2	2.84	3.00	3.19	3.31	3.46	3.66
	Mo–S	2.37	2.38	2.41	2.45	2.49	2.53
Average bond angle (°)	Mo_1–S_1–Mo_2	74.17	78.21	82.30	85.28	88.60	91.29
	S_1–Mo_2–S_2	74.32	78.28	82.30	85.08	88.54	90.89
	S_1–Mo_1–S_3	91.66	87.65	80.54	79.42	73.07	70.98

Table 3 The structural parameters of PEI under the variation of lattice constant. See Fig. 5 for the atom index of PEI

a (Å)		2.84	3.00	3.18	3.32	3.48	3.64
Bond length (Å)	N_y–C_5	1.425	1.437	1.467	1.494	1.525	1.519
	N_y–C_4	1.427	1.438	1.462	1.484	1.501	1.486
	N_y–C_7	1.443	1.451	1.471	1.488	1.498	1.483
	N_1–C_1	1.457	1.459	1.465	1.494	1.468	1.455
	N_2–C_2	1.450	1.444	1.461	1.472	1.486	1.474
	N_2–C_3	1.436	1.451	1.463	1.478	1.488	1.469
	N_3–C_6	1.459	1.461	1.464	1.470	1.469	1.459
	N_4–C_8	1.458	1.460	1.463	1.466	1.461	1.448
	C_7–C_8	1.509	1.519	1.543	1.570	1.615	1.635
	C_3–C_4	1.512	1.524	1.538	1.556	1.591	1.599
	C_5–C_6	1.508	1.514	1.537	1.558	1.588	1.578
Bond angle (°)	$C_6C_5N_y$	111.32	113.10	116.54	119.13	122.96	123.74
	$C_4C_3N_2$	110.41	112.37	115.27	117.23	118.62	118.63
	$C_8C_7N_y$	109.56	110.63	113.54	115.63	119.09	119.27
	$C_3C_4N_y$	109.81	111.11	115.02	117.74	121.79	122.44
	$C_3N_2C_2$	109.57	112.15	116.40	119.52	123.78	126.79
	$C_5N_yC_4$	113.45	113.52	114.45	115.11	116.75	116.77
	$C_7N_yC_4$	112.10	113.19	113.98	114.69	116.59	118.82
	$C_7N_yC_5$	111.90	110.93	111.71	112.22	113.97	111.86

varying the lattice constant a while remaining the slab thickness.

Optical properties were determined through the frequency-dependent complex dielectric function, $\varepsilon(\omega) = \varepsilon_1(\omega) + i\varepsilon_2(\omega)$[21,38] which is the measure of the light absorption and emission of material. The imaginary part of the dielectric constant $\varepsilon_2(\omega)$ was computed by using the following expression:[38]

$$\varepsilon_2(\omega) = \frac{2\pi e^2}{V\varepsilon_0}\sum_{k,v,c}\left|\left\langle\psi_k^c|\hat{u}\cdot r|\psi_k^v\right\rangle\right|^2\delta\left[E_k^c - E_k^v - \hbar\omega\right], \quad (3)$$

where ω is the frequency of light, ε_0 is the dielectric constant of vacuum. ψ_k^c and ψ_k^v are the conduction and valence band wave functions, respectively. V is the volume of the unit cell and $\hat{u}$ is the vector defining the polarization of the electric field of the incident light. The real part $\varepsilon_1(\omega)$ can be calculated through $\varepsilon_2(\omega)$ using the Kramer–Kronig relation,

$$\varepsilon_1(\omega) = 1 + \left(\frac{2}{\pi}\right)\int_0^\infty d\omega' \frac{(\omega')^2\varepsilon_2(\omega)}{(\omega')^2 - \omega^2}. \quad (4)$$

2. Results and discussion

2.1. The adsorption of the PEI fragment on the monolayer MoS_2

We have to perform the geometric optimization of the monolayer MoS_2 before the study of the PEI adsorption. The lattice constant of the monolayer MoS_2 was optimized by the GGA-PBE method and obtained the parameters of $a = b = 3.18$ Å. The average bond length of Mo–S is 2.42 Å. The S–Mo–S and Mo–S–Mo angles are 82.30°. The thickness of the triple atomic layers of MoS_2 is 3.13 Å. These results are in good agreement with the previous experimental and theoretical studies.[23,39,40]

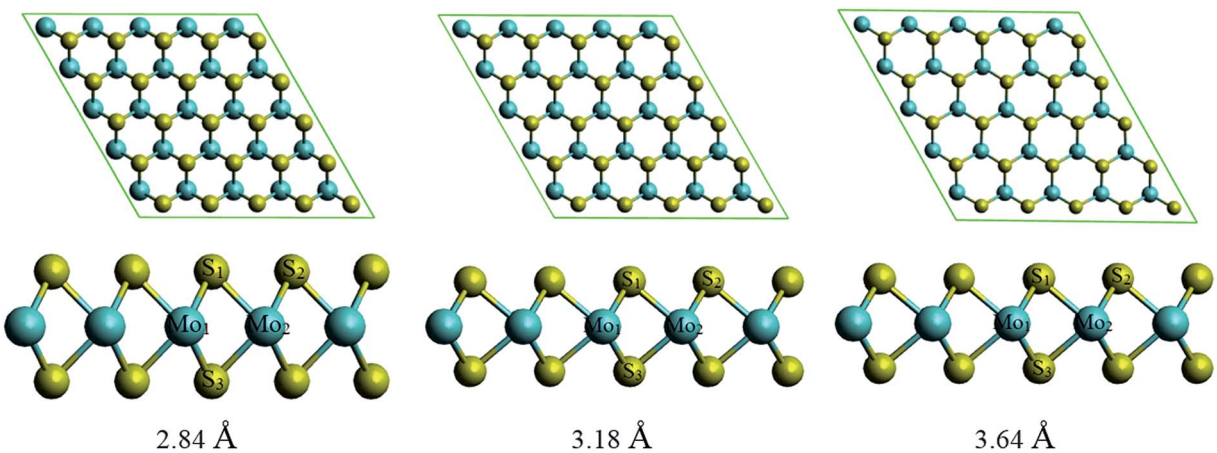

Fig. 4 The upper and lower panels are the top and side views of the MoS_2 slab with the change of lattice constant, respectively.

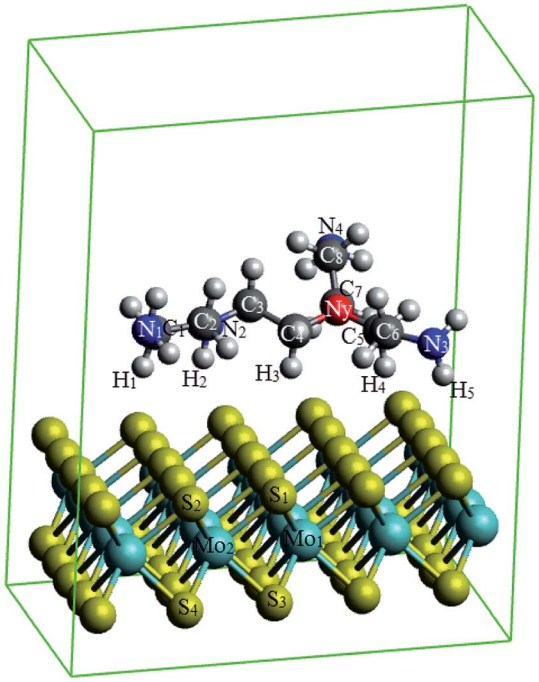

Fig. 5 The atom index of PEI on MoS_2.

To study the influences of the pressure, we varied the lattice constant with the constraint $a = b$ of the clean MoS_2 and the MoS_2/PEI system and explored the differences of two systems before and after changing the lattice constant. We considered the following values of the lattice constant: 2.84, 3.00, 3.18, 3.32, 3.48, and 3.64 Å. Two first values correspond to compressive strains and three last values correspond to the tensile strains.

The MoS_2/PEI system was prepared by loading the PEI fragment on the optimized monolayer MoS_2. The MoS_2/PEI system was allowed to fully relax for every step of the calculations. The PEI fragment was initially placed parallel to the surface of the monolayer MoS_2 with a vertical distance of around 3.5 Å. Since the stability of the PEI adsorption correlates to the number of nitrogen atoms associated with the surface of the substrate, the stable geometry of the MoS_2/PEI system was obtained with a flat structure of the PEI fragment on the surface of the monolayer MoS_2. We considered several possible adsorption sites of the PEI molecule on the surface of MoS_2, see Fig. 2. After performing the geometric optimization, we obtained the optimized structures of MoS_2/PEI with the total energies of −741.39, −741.38, −741.43, and −741.41 eV for those in Fig. 2a–d, respectively. Based on these energies, we found the most favorable adsorption configuration of the PEI molecule as the N atom with three alkyl groups, denoted as N_y, positioned on the top of the S atom (Fig. 2c). The average vertical distance from the lowest nitrogen atoms, the lowest carbon atoms and the lowest hydrogen atoms of PEI to the surface of the substrate are 3.63, 3.76, and 2.37 Å, respectively.

We now perform the structural optimization for each variation of the lattice constant for the most favorable adsorption

Table 4 The bandgap of MoS_2 and MoS_2/PEI

	MoS_2		MoS_2/PEI	
a (Å)	P (GPa)	E_g (eV)	P (GPa)	E_g (eV)
2.84	−56.18	1.05	−50.48	0.53
3.00	−32.44	1.55	−38.51	0.81
3.04	−27.65	1.72	−22.44	0.83
3.12	−10.69	1.80	−11.94	0.82
3.16	−9.46	1.75	−8.12	0.69
3.18	0	1.68	0	0.55
3.20	1.53	1.61	0.95	0.46
3.24	5.04	1.29	5.74	0.02
3.32	10.13	0.81	10.25	0.01
3.48	24.95	0	21.79	0
3.64	41.14	0	31.62	0

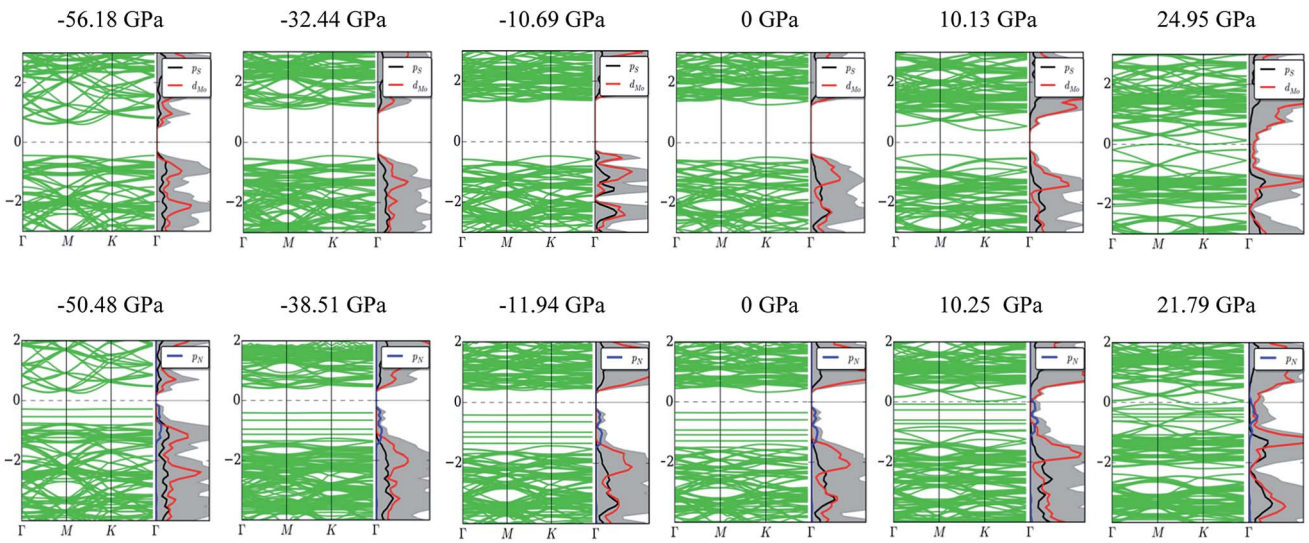

Fig. 6 The band structure and total density of states of MoS_2 (upper panel) and MoS_2/PEI (lower panel) with the variation of pressure.

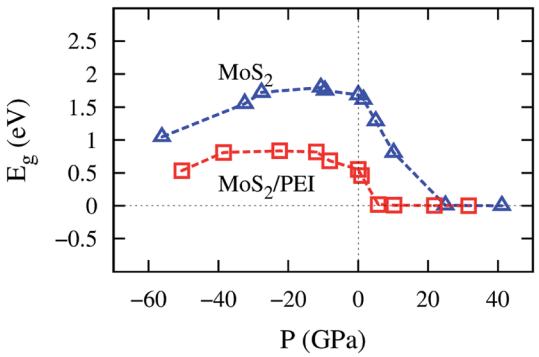

Fig. 7 The bandgap *versus* pressure of MoS_2 and MoS_2/PEI.

configuration of the PEI molecule on the MoS_2 substrate. The adsorption energy of the PEI fragment on the substrate and the distances from this molecule to the substrate are listed in Table 1. We found that the distances increase slightly with the increase of the lattice constant.

Furthermore, Fig. 3 shows that the adsorption energy becomes more negative; and hence, the favorable order of the PEI adsorption increases with the increase of the lattice constant. For the compression, with the lattice constant $a < 3.18$ Å, the adsorption energy is positive, which indicates that the adsorption of the PEI molecule is unstable on the surface of the monolayer MoS_2. In contrast, for the cases of without strain ($a = 3.18$ Å) and tensile strains ($a > 3.18$ Å), the adsorption energy is negative. This result implies that the adsorption of the PEI molecule is stable. We found that the higher the lattice constant, the stronger the PEI molecule adsorbs. However, the interaction between the PEI molecule and the monolayer MoS_2 is weak and the PEI molecule physisorbed on the MoS_2. Furthermore, the phonon vibrational energy of the stretching mode of PEI is 0.43 eV. This value is comparable to the adsorption energy of PEI; therefore, the adsorption of PEI is thermodynamically unstable except for applying a high enough tensile pressure to the MoS_2/PEI system.

The structural information was shown in Table 2 for MoS_2 and Table 3 for PEI with the change of lattice constant. We found that the average bond length between S_1–S_2, Mo–Mo, Mo–S, and the average bond angles Mo_1–S_1–Mo_2, S_1–Mo_2–S_2 increase, while the thickness of the MoS_2 slab shown by S_1–S_3 and also the angle S_1–Mo_1–S_3 decrease with the increase of lattice constant. Although the structural parameters for the MoS_2 monolayer have been modified, the MoS_2 monolayer under pressure remains the 2H phase similar to that of without strain. We can confirm this information by Fig. 4, where the top view of the MoS_2 shows the honeycomb structure and the side views exhibit a similar structure for all considering lattice constants of 2.84, 3.18, and 3.64 Å. Table 3 shows the structural information of PEI that the bond lengths of N–C and C–C, and the bond angles of C–C–N and C–N–C somehow increase with the increase of the lattice constant.

2.2. Effects of the PEI adsorption and pressure on electronic structure properties of MoS_2

The effects of the PEI adsorption and the pressure variation by changing $a = b$ on the electronic properties of the monolayer MoS_2 were elucidated through the band structure, the density of states (DOS), and the charge exchange of the systems before and after these factors taking place.

Fig. 6 shows that, at zero pressure, the monolayer MoS_2 has a direct bandgap of 1.68 eV at the K point in the Brillouin zone, which is in good agreement with the previous publications.[4,32,41] The total electronic density of states shows that the valence band maximum (VBM) and the conduction band minimum (CBM) are contributed mainly by Mo-4d states and weakly by S-3p states. The adsorption of the PEI molecule makes the energy levels of the MoS_2/PEI system lower than that of the isolated monolayer MoS_2, simultaneously creates new flat energy levels in the bandgap region which significantly decreases the direct bandgap of the monolayer MoS_2 to 0.55 eV. The new energy levels appear in the region of the valence band of MoS_2/PEI implying that the monolayer MoS_2 became an n-type semiconductor upon the adsorption of the PEI molecule. The new flat energy levels mainly come from the contribution of the N-2p lone pair. Notably, at non-zero pressures, the bandgap of MoS_2 and MoS_2/PEI becomes narrower than that at zero pressure and gradually approaches 0 eV at some specific values of the pressure. When MoS_2 and MoS_2/PEI still show the semiconductor property, the significant difference between the electronic properties of two systems is that the bandgap of MoS_2 changes from direct to indirect upon the variation of pressure, while

Table 5 The Bader charge (*e*) for the MoS_2/PEI system: (+) charge gain, (−) charge loss. The electrostatic force (e^2 Å^{-1}) between the H, C, and N atoms of the PEI with the S atoms of the MoS_2 denotes by F_1, F_2, and F_3, respectively. The negative and positive signs of the force imply the attraction and repulsion, respectively. The total force $F = F_1 + F_2 + F_3$

	MoS_2/PEI											
P (GPa)	23H	8C	5N	25Mo	50S	PEI	MoS_2	E_g (eV)	F_1	F_2	F_3	F
−50.48	−1.62	−3.21	4.79	−40.27	40.32	−0.05	0.05	0.53	−28.97	−35.66	54.67	−9.96
−38.51	−1.91	−3.09	4.96	−43.45	43.48	−0.04	0.04	0.81	−36.07	−36.08	60.41	−11.74
0	−1.94	−3.11	5.01	−43.66	43.70	−0.04	0.04	0.55	−35.84	−36.14	60.32	−11.67
10.25	−1.95	−3.10	4.92	−43.27	43.40	−0.13	0.13	0.01	−34.95	−35.30	57.99	−12.25
21.79	−2.52	−2.97	5.07	−42.85	43.27	−0.42	0.42	0	−44.24	−33.16	58.80	−18.60
31.62	−2.76	−3.06	5.24	−42.01	42.59	−0.58	0.58	0	−46.76	−33.21	58.26	−21.71

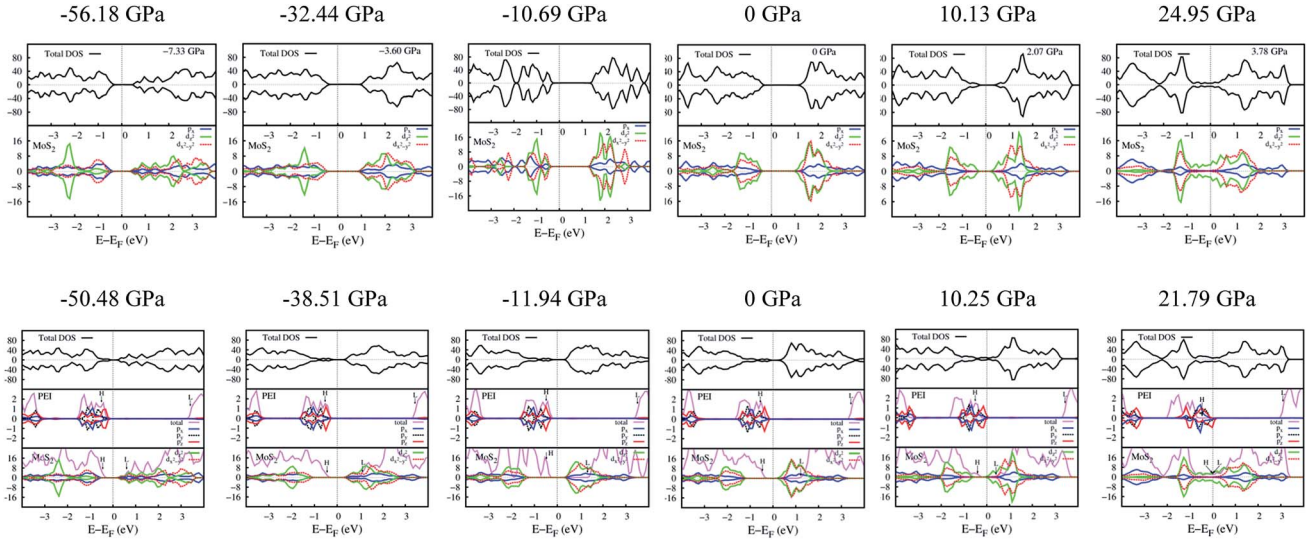

Fig. 8 Total and projected DOS of MoS_2 (upper panel) and MoS_2/PEI (lower panel).

MoS_2/PEI remains direct bandgap with a smaller value due to the flat characteristics of the new energy levels but at a different position of the *k*-point mesh.

The pressure correspondence to the variation of the lattice constant of the MoS_2 and MoS_2/PEI systems was calculated by using the expression (2). The detailed values of the bandgap *versus* the pressure and the lattice constant were listed in Table 4. We found that the pressure varies from −56.18 to 41.14 GPa and −50.48 to 31.62 GPa for the lattice constant from 2.84 to 3.64 Å for the MoS_2 and MoS_2/PEI systems, respectively. The negative and positive signs represent the compressive and tensile strains in that order. We see that the pressure scale for the isolated MoS_2 is similar to that for the MoS_2/PEI system at the same value of the lattice constant.

The bandgap *versus* the pressure is visualized in Fig. 7. We found that the behavior of the bandgap for the isolated MoS_2 is similar to that for MoS_2/PEI, which is a parabola with a maximum value of 1.80 and 0.83 eV at the pressure of −10.69 and −22.44 GPa for the isolated MoS_2 and MoS_2/PEI systems, respectively. Furthermore, when the tensile pressure approaches 24.95 and 21.79 GPa, the bandgap approaches 0 eV for these systems in that order. This result implies that the monolayer MoS_2 and MoS_2/PEI systems transit from semiconductor to metal at the obtained values of the tensile pressure. The transition was found to be a little easier for the MoS_2/PEI than the monolayer MoS_2. The parabolic behavior of the bandgap is in good agreement with the experiment for the isolated MoS_2.[16]

The amount of the charge exchange between the monolayer MoS_2 and the PEI fragment was presented by the Bader point charge in Table 5. The plus and minus signs denote the charge gain and loss, respectively. Particularly, the hydrogen and carbon atoms donate while the nitrogen atoms gain charge. The total outcome is that the PEI molecule donates and the MoS_2 gains charge. The charge exchange was found to inversely proportional to the bandgap. The higher the charge exchange, the narrower the bandgap becomes. This result supports the nature of the n-type doping to the substrate by the PEI polymer.

In common sense, a simple adsorbate will approach the substrate surface as its adsorption energy becomes more negative. However, for the complicated structure as the PEI molecule, as shown in Table 1, the distances from the nearest N, C, and H atoms of PEI to the surface of the MoS_2 monolayer exhibit that the PEI molecule is slightly moving away from the surface as the lattice constant increases with the more negative

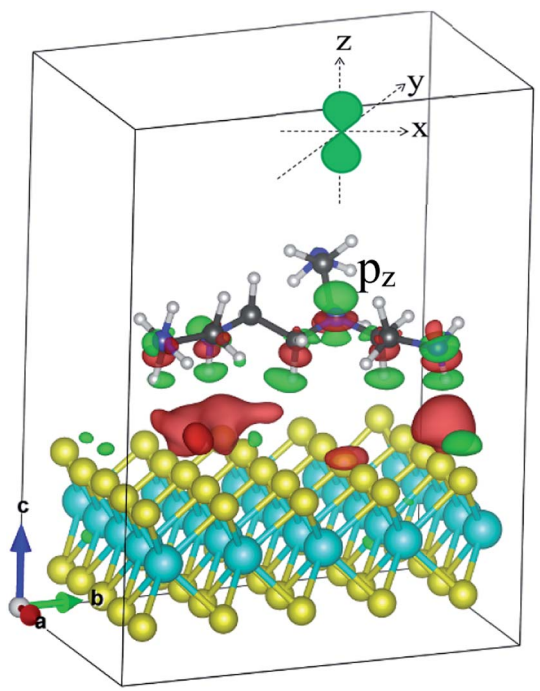

Fig. 9 The charge density difference of the MoS_2/PEI system. Occupied and unoccupied states are presented in red and green, respectively.

Table 6 The HOMO of isolated PEI and the LUMO of isolated MoS_2

	a (Å)	2.84	3.00	3.12	3.16	3.18	3.32	3.48	3.64
Isolated PEI	HOMO (eV)	−0.51	−0.53	−0.49	−0.53	−0.56	−0.51	0.00	0.00
Isolated MoS_2	LUMO (eV)	0.60	1.11	1.32	1.27	1.22	0.40	0.00	0.00
LUMO–HOMO (eV)		1.11	1.64	1.81	1.80	1.78	0.91	0.00	0.00

adsorption energy. This observation seems to be contradicted; however, it can be explained in terms of the attractive electrostatic force between the PEI and the MoS_2, which increases with the increase of the lattice constant. As shown in Table 5, the attractive force was found for the pairs of H–S and C–S and the repulsive force for the pairs of N–S atoms. The N–S repulsive force is strong enough to win the H–S and C–S attractive forces; and hence, it somehow lifts the whole PEI molecule away from the MoS_2 surface. However, the total electrostatic force F remains the increasing attractive property with an increase in the pressure. The increasing attractive property of the total force is attributed mainly to the increase of the attractive interaction of the H atoms with the S atoms.

Fig. 8 presents the total DOS and the orbital projected DOS of the monolayer MoS_2 and MoS_2/PEI systems. At zero pressure, the total DOS exhibits a high symmetry of spin-up and spin-down components implying the non-magnetic properties of both MoS_2 and MoS_2/PEI systems. For the negative pressures, the projected DOS of the monolayer MoS_2 shows that the contribution to the VBM and CBM is attributed to the $d_{x^2-y^2}$ orbital of the Mo atoms and the p_x state of the S atoms. For the pressure ≥ 0, the d_{z^2} orbital becomes dominant for the energy range near the Fermi level. The adsorption of the PEI molecule contributes to the occurrence of the new states, which comes from the contribution of the p_z states of the N atoms. We can see more details in Fig. 9, the charge clouds of the N_y nitrogen atoms clearly exhibit the shape of the p_z orbitals. The charge donation and accumulation distribute on the PEI fragment and the surface of the MoS_2, respectively. This result is in good agreement with the behavior of the Bader point charge.

The parabolic behavior of the bandgap, as shown in Fig. 7, is attributed to the different responses of the $d_{x^2-y^2}$ and d_{z^2} orbitals of the MoS_2 monolayer toward the pressure, see Fig. 8 (upper panel). At the negative pressures, the $d_{x^2-y^2}$ orbital plays the main role, while at the higher pressures, the d_{z^2} orbital gradually becomes dominant at the VBM and CBM. The contribution from these orbitals is balanced at the VBM and CBM; and hence, the bandgap is broadest for the pressure of −10.69 GPa. When the d_{z^2} orbital approaches the Fermi level, the bandgap becomes narrower, as the tensile pressure increases. Furthermore, the study of HOMO and LUMO can support the understanding of the interaction between the MoS_2 substrate and the PEI adsorbate; and hence, the parabolic behavior of the MoS_2/PEI bandgap. We presented the HOMO and LUMO states of the isolated MoS_2 and isolated PEI in Fig. 8 (lower panel). The values of the MoS_2 LUMO and the PEI HOMO were also listed in Table 6. We found that the HOMO–LUMO gap varies with the parabolic behavior as that of the bandgap of the MoS_2/PEI system (Fig. 7), which increases first and then decreases with the increase of the pressure from the negative to the positive value.

2.3. Optical properties of MoS_2 and MoS_2/PEI

In this section, we studied the effects of the PEI adsorption and the pressure on the optical properties of the monolayer MoS_2. The imaginary dielectric function $\varepsilon_2(\omega)$ of MoS_2 and MoS_2/PEI systems were calculated through the expression (3) and shown in Table 7. The photon wavelength was calculated by using the formula $\lambda = hc/E_p$, where h is the Planck constant, c is the speed of light in vacuum, and E_p is the photon energy. The obtained result is listed in the third and seventh columns of Table 7.

As shown in Fig. 10a, at $P = 0$ GPa, the photoluminescence spectrum of the monolayer MoS_2 exhibits the main peak at 453 nm within the range of visible light (400–800 nm). The result indicates that the MoS_2 can absorb and emit the blue light, which is in agreement with the previous report.[22,32] At non-zero pressures, the main PL peak shifts to the longer wavelength and simultaneously suppresses the peak height compared to that at zero pressure. Besides, for the positive pressure, the main peak tends to separate into two peaks. Furthermore, the intensity of the maximum PL is lower for the negative pressure than the positive pressure. We also found new peaks in the

Table 7 The wavelength and dielectric function at the maximum intensity of photoluminescence

	MoS_2					MoS_2/PEI			
P (GPa)	E_g (eV)	E_p (eV)	λ (nm)	$\varepsilon_2(\omega)$	P (GPa)	E_g (eV)	E_p (eV)	λ (nm)	$\varepsilon_2(\omega)$
−56.18	1.05	4.66	266	11.06	−50.48	0.53	4.61	269	9.98
−32.44	1.55	2.60	477	11.58	−38.51	0.81	2.76	449	11.10
0	1.68	2.73	453	14.88	0	0.55	2.72	456	14.91
10.13	0.81	2.39	521	13.36	10.25	0.01	2.35	527	13.38
24.95	0	2.00	621	13.18	21.79	0	2.01	618	12.86
41.14	0	1.42	873	12.06	31.62	0	1.41	877	11.12

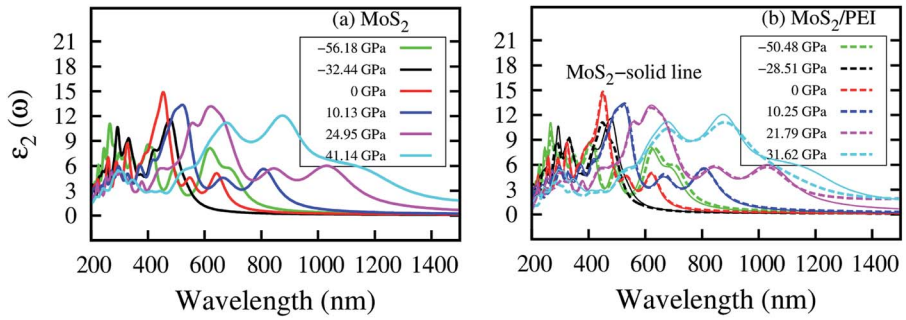

Fig. 10 Imaginary dielectric function $\varepsilon_2(\omega)$ *versus* wavelength for MoS_2 (a) and MoS_2/PEI (b).

photoluminescence of the isolated MoS_2 occurring in the ultraviolet region upon the compression and in the infrared region upon the tensile strain. The photoluminescence spectrum of the MoS_2/PEI system in Fig. 10b remains almost unchanged compared to that of the isolated MoS_2. This result implies that the benefit of the PEI coating is not only to protect the MoS_2 from the adsorption of the unexpected gases but also remain the optical properties of the MoS_2, which can be used for various optoelectronic applications.

3. Conclusion

In this paper, we have studied the electronic and optical properties of the monolayer MoS_2 under the influences of the polyethyleneimine adsorption and the pressure. We found that the bandgap of the monolayer MoS_2 reduces significantly upon the PEI adsorption, which was attributed to the p_z state of the nitrogen atoms occurring in the bandgap region. The bandgap of MoS_2 and MoS_2/PEI systems approaches 0 eV at the tensile pressure of 24.95 and 21.79 GPa, respectively. The pressure also modifies the photoluminescence spectrum of the monolayer MoS_2 and MoS_2/PEI systems as shifting the main peak to the longer wavelength. Particularly, the compression and tensile strain generate new peaks in the ultraviolet and infrared regions, respectively. However, the PEI adsorption does not significantly alter the characteristics of the photoluminescence spectrum of the monolayer MoS_2 at all pressure ranges. The coating of the polyethyleneimine does not only protect the monolayer MoS_2 from the sensitive gases but also remain the optical properties of this system. This result is perhaps useful for the utilization of the MoS_2/PEI in optoelectronic devices.

Conflicts of interest

There are no conflicts of interest to declare.

Acknowledgements

This research was funded by the Ho Chi Minh City Department of Science and Technology under contract number 310/QĐ-KHCNTT (2018). We acknowledge the usage of the computer time and software granted by the Institute of Physical Chemistry of Romanian Academy, Bucharest (HPC infrastructure developed under the projects Capacities 84 Cp/I of 15.09.2007 and INFRANANOCHEM 19/01.03.2009).

References

1 H. Zeng, J. Dai, W. Yao, D. Xiao and X. Cui, Valley polarization in MoS_2 monolayers by optical pumping, *Nat. Nanotechnol.*, 2012, **7**(8), 490–493.
2 A. Enyashin and G. Seifert, Electronic properties of MoS_2 monolayer and related structures, *Nanosyst.: Phys., Chem., Math.*, 2014, **5**(4), 517–539.
3 A. Castellanos-Gomez, M. Poot, G. A. Steele, H. S. J. van der Zant, N. Agraït and G. Rubio-Bollinger, Elastic properties of freely suspended MoS_2 nanosheets, *Adv. Mater.*, 2012, **24**(6), 772–775.
4 K. F. Mak, C. Lee, J. Hone, J. Shan and T. F. Heinz, Atomically thin MoS_2: a new direct-gap semiconductor, *Phys. Rev. Lett.*, 2010, **105**, 136805.
5 B. Radisavljevic, A. Radenovic, J. Brivio, V. Giacometti and A. Kis, Single-layer MoS_2 transistors, *Nat. Nanotechnol.*, 2011, **6**, 147–150.
6 Y. Yu, F. Miao, J. He and Z. Ni, Photodetecting and Light-Emitting Devices Based on Two Dimensional Materials, *Chin. Phys. B*, 2017, **26**, 036801.
7 J. Martincová, M. Otyepka and P. Lazar, Is Single Layer MoS_2 Stable in the Air?, *Chem.–Eur. J.*, 2017, **23**, 13233–13239.
8 Y. Du, H. Liu, A. T. Neal, M. Si and P. D. Ye, Molecular Doping of Multilayer MoS_2 Field-Effect Transistors: Reduction in Sheet and Contact Resistances, *IEEE Electron Device Lett.*, 2013, 0741–3106.
9 S. Hong, G. Yoo, D. H. Kim, W. G. Song, O. K. Le, Y. Ki Hong, K. Takahashi, I. Omkaram, D. N. Son and S. Kim, The doping mechanism and electrical performance of polyethylenimine-doped MoS_2 transistor, *Phys. Status Solidi C*, 2017, 1600262.
10 M. Chhowalla, H. S. Shin, G. Eda, L.-J. Li, K. P. Loh and H. Zhang, The chemistry of two-dimensional layered transition metal dichalcogenide nanosheets, *Nat. Chem.*, 2013, **5**(4), 263–275.
11 L. Yang, X. D. Cui, J. Zhang, K. Wang, M. Shen, S. Zeng, S. A. Dayeh, L. Feng and B. Xiang, Lattice strain effects on the optical properties of MoS_2 nanosheets, *Sci. Rep.*, 2014, **4**, 5649.

12 P. Johari and V. B. Shenoy, Tuning the Electronic Properties of Semiconducting Transition Metal Dichalcogenides by Applying Mechanical Strains, *ACS Nano*, 2012, **6**(6), 5449–5456.
13 Q. Yue, J. Kang, Z. Shao, X. Zhang, S. Chang, G. Wang, S. Qin and J. Li, Mechanical and electronic properties of monolayer MoS_2 under elastic strain, *Phys. Lett. A*, 2012, **376**, 1166–1170.
14 X. Fan, C.-H. Chang, W. T. Zheng, J.-L. Kuo and D. J. Singh, The Electronic Properties of Single-Layer and Multilayer MoS_2 under High Pressure, *J. Phys. Chem. C*, 2015, **119**, 10189–10196.
15 F. Li, Y. Yan, B. Han and T. Cui, Pressure confinement effect in MoS_2 monolayers, *Nanoscale*, 2015, **7**(19), 1–8.
16 M. López-Suárez, I. Neri and R. Rurali, Bandgap engineering of MoS_2 upon compression, *J. Appl. Phys.*, 2016, **119**, 165105.
17 X. Dou, K. Ding, D. Jiang and B. Sun, Tuning and Identification of Interband Transitions in Monolayer and Bilayer Molybdenum Disulfide Using Hydrostatic Pressure, *ACS Nano*, 2014, **8**(7), 7458–7464.
18 Y. Y. Hui, X. Liu, W. Jie, N. Y. Chan, J. Hao, Y. T. Hsu, L. J. Li, W. Guo and S. P. Lau, Exceptional tunability of band energy in a compressively strained trilayer MoS_2 sheet, *ACS Nano*, 2013, **7**(8), 7126–7131.
19 A. P. Nayak, T. Pandey, D. Voiry, J. Liu, S. T. Moran, A. Sharma, C. Tan, C.-H. Chen, L.-J. Li, M. Chhowalla, J.-F. Lin, A. K. Singh and D. Akinwande, Pressure-Dependent Optical and Vibrational Properties of Monolayer Molybdenum Disulfide, *Nano Lett.*, 2015, **15**(1), 346–353.
20 X. Cheng, Y. Li, J. Shang, C. Hu, Y. Ren, M. Liu and Z. Qi, Thickness-dependent phase transition and optical behavior of MoS_2 films under high pressure, *Nano Res.*, 2018, **11**, 855–863.
21 J. Shang, L. Zhang, X. Cheng and F. Zhai, Pressure induced effects on the electronic and optical properties of MoS_2, *Solid State Commun.*, 2015, **219**, 33–38.
22 Z. Yin, H. Li, H. Li, L. Jiang, Y. Shi, Y. Sun, G. Lu, Q. Zhang, X. Chen and H. Zhang, Single-Layer MoS_2 Phototransistors, *ACS Nano*, 2011, **6**(1), 74–80.
23 Y. Jing, X. Tan, Z. Zhou and P. Shen, Tuning electronic and optical properties of MoS_2 monolayer *via* molecular charge transfer, *J. Mater. Chem. A*, 2014, **2**, 16892–16897.
24 S. Mouri, Y. Miyauchi and K. Matsuda, Tunable Photoluminescence of Monolayer MoS_2 *via* Chemical Doping, *Nano Lett.*, 2013, **13**(12), 5944–5948.
25 Y. Wang, A. Slassi, M.-A. Stoeckel, S. Bertolazzi, J. Cornil, D. Beljonne and P. Samorì, Doping of Monolayer Transition-Metal Dichalcogenides *via* Physisorption of Aromatic Solvent Molecules, *J. Phys. Chem. Lett.*, 2019, **10**(3), 540–547.
26 R. C. Selhorst, E. Puodziukynaite, J. A. Dewey, P. Wang, M. D. Barnes and A. R. T. Emrick, Tetrathiafulvalene-containing polymers for simultaneous non-covalent modification and electronic modulation of MoS_2 nanomaterials, *Chem. Sci.*, 2016, **7**, 4698–4705.
27 G. Kresse and J. Hafner, *Ab initio* molecular dynamics for open-shell transition metals, *Phys. Rev. B: Condens. Matter Mater. Phys.*, 1993, **48**, 13115–13118.
28 G. Kresse and J. Hafner, *Ab initio* molecular-dynamics simulation of the liquid-metal– amorphous-semiconductor transition in germanium, *Phys. Rev. B: Condens. Matter Mater. Phys.*, 1994, **49**, 14251–14269.
29 G. Kresse and J. Furthmuller, Efficient iterative schemes for *ab initio* total-energy calculations using a plane-wave basis set, *Phys. Rev. B: Condens. Matter Mater. Phys.*, 1996, **54**, 11169–11186.
30 J. P. Perdew, J. A. Chevary, S. H. Vosko, K. A. Jackson, M. R. Pederson, D. J. Singh and C. Fiolhais, Atoms, molecules, solids, and surfaces: applications of the generalized gradient approximation for exchange and correlation, *Phys. Rev. B: Condens. Matter Mater. Phys.*, 1992, **46**, 6671.
31 J. P. Perdew, K. Burke and M. Ernzerhof, Generalized Gradient Approximation Made Simple, *Phys. Rev. Lett.*, 1996, **77**, 3865.
32 Y. Li, Y.-L. Li, C. M. Araujo, W. Luo and R. Ahuja, Single-layer MoS_2 as an efficient photocatalyst, *Catal.: Sci. Technol.*, 2013, **3**, 2214.
33 P. E. Blochl, Projector augmented-wave method, *Phys. Rev. B: Condens. Matter Mater. Phys.*, 1994, **50**, 17953.
34 G. Kresse and J. Joubert, From ultrasoft pseudopotentials to the projector augmented-wave method, *Phys. Rev. B: Condens. Matter Mater. Phys.*, 1999, **59**, 1758.
35 H. J. Monkhorst and J. D. Pack, Special points for Brillouin-zone integrations, *Phys. Rev. B: Solid State*, 1976, **13**, 5188–5192.
36 J. Neugebauer and M. Scheffler, Adsorbate-substrate and adsorbate-adsorbate interactions of Na and K adlayers on Al(111), *Phys. Rev. B: Condens. Matter Mater. Phys.*, 1992, **46**, 16067–16080.
37 L. Bengtsson, Dipole correction for surface supercell calculations, *Phys. Rev. B: Condens. Matter Mater. Phys.*, 1999, **59**, 12301–12304.
38 L. J. Kong, G. H. Liu and L. Qiang, Electronic and optical properties of O-doped monolayer MoS_2, *Comput. Mater. Sci.*, 2016, **111**, 416–423.
39 N. Wakabayashi, H. G. Smith and R. M. Nicklow, Lattice dynamics of hexagonal MoS_2 studied by neutron scattering, *Phys. Rev. B: Solid State*, 1975, **12**, 659.
40 Y. Li, Z. Zhou, S. Zhang and Z. Chen, MoS_2 Nanoribbons: High Stability and Unusual Electronic and Magnetic Properties, *J. Am. Chem. Soc.*, 2008, **130**, 16739–16744.
41 A. Splendiani, L. Sun, Y. Zhang, T. Li, J. Kim, C.-Y. Chim, G. Galli and F. Wang, Emerging Photoluminescence in Monolayer MoS_2, *Nano Lett.*, 2010, **10**, 1271.

